Accepted Article Preview: Published ahead of online publication

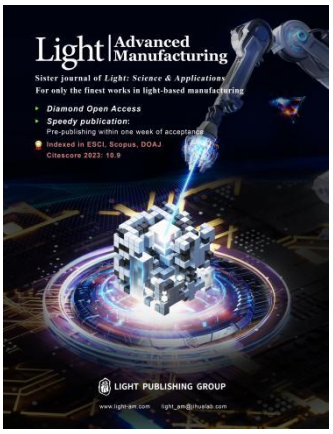

Reusable Plasmonic Au and Ag Diamond Films for Robust SERS Sensing

Kieran N. Twaddle, Massimiliano L.A. Ramsay, Richard B. Jackman

Cite this article as: Kieran N. Twaddle, Massimiliano L.A. Ramsay, Richard B. Jackman. Reusable Plasmonic Au and Ag Diamond Films for Robust SERS Sensing. *Light: Advanced Manufacturing* accepted article preview 1 July, 2026; doi: 10.37188/lam.2026.115

Received 29 November 2025; Revised 27 June 2026; Accepted 1 July 2026; Accepted article preview online 1 July 2026

Reusable Plasmonic Au and Ag Diamond Films for Robust SERS Sensing

Kieran N. Twaddle[1], Massimiliano L.A. Ramsay[1], and Richard B. Jackman[1]

[1]London Centre for Nanotechnology and the Department of Electronic and Electrical Engineering, UCL (University College London), 17-19 Gordon Street, London, WC1H 0AH, UK

Correspondance: Kieran N. Twaddle (kieran.twaddle.22@ucl.ac.uk) | Richard B. Jackman (r.jackman@ucl.ac.uk)

Funding: Engineering and Physical Sciences Research Council (EPSRC) of the UK and SLB Cambridge Research Ltd, Grant/Award Number: EP/W524335/1

ABSTRACT

Surface-enhanced Raman Spectroscopy (SERS) is an excellent technique for chemical identification, capable of trace level detection which is vital in a wide variety of fields. However, SERS measurements are restricted to the laboratory environment, requiring a specialised setup and fragile, ordinarily single-use, plasmonic substrates. To enable rugged and reusable SERS measurements, a robust and chemically stable plasmonic substrate is required. Diamond possesses ideal properties for this application and, crucially, can be grown in a laboratory, enabling the incorporation of plasmonic nanostructures within a diamond film. Robust SERS substrates have been fabricated by encapsulating both Ag and Au nanoparticles (NPs) in thin diamond films. Diamond growth conditions provides control over the resulting plasmonic properties, allowing for comparison and optimised parameter determination. Investigation of Ag and Au-NPs 2-75 nm in diameter with diamond film thicknesses of 0 to ∼100 nm provided diverse diamond overgrowth interactions and SERS enhancement leading to optimised practical results. Using optimal fabrication parameters, a peak enhancement of EF = 6.9 $\times 10^3$ was obtained with a 1×10^{-5} M limit of detection. Additionally, no reduction in SERS performance was observed after a regime of harsh treatments (sonication, metal etchant, physical abrasion, 400℃ anneal), evidencing the robust and reusable nature of this approach.

Keywords: Metallic Nanoparticles, Diamond, Surface Enhanced Raman Spectroscopy, Plasmonics, Thin film

Introduction

Diamond has excellent physical qualities, including the highest bulk modulus and extreme mechanical hardness, allowing application in virtually any environment[1]. Given this, diamond is suitable for employment in extreme environments which may exhibit high pressure, high temperature, physical abrasion, chemical harshness or even radiation. Embedding structures within diamond facilitates techniques in these environments which were previously inaccessible. Metallic nanoparticles (NPs) are one example of an embeddable structure, realising enhanced light-matter interactions in harsh environments for a number of fields such as photocatalysis, photovoltaics, and quantum sensing.

Surface-Enhanced Raman Spectroscopy (SERS) is a notable example which utilises NP plasmonic interactions. This technique allows for trace level chemical identification in complex sample compositions. However, conventional SERS measurements are restricted to the laboratory environment due to the fragile nature of the plasmonic nanostructures required. The NPs are commonly fabricated on paper or opaque silicon surfaces where the NPs are exposed to analyte[2,3]. These substrates suffer from longevity issues with respect to lack of multi-measurement capabilities and short shelf lives. Therefore, to enable SERS application in real world environments or increase substrate longevity, a robust and chemically stable plasmonic substrate is required. Some progress towards this goal has been made, with a steel wire mesh[4], SiO_2 coatings[5], nickel foam-cages[6], copper foam coatings[7], and boron nitride coatings[8] having been presented. Each of these approaches addresses aspects of SERS fragility, however, a fully all-round substrate which is physically, chemically and thermally robust is yet to be reported.

A limited number of studies have reported overgrowing common metallic NPs of Ag and Au with diamond for alternate applications. Ag-NPs have been embedded in diamond films by both Li *et al.* and Bellucci *et al.* with NP diameters ranging from 10-500 nm and diamond films 20-400 nm thick for photocatalytic activity[9,10], quantum-based sensing[11], and film colour tunability[12]. Incorporation of the plasmonic NPs provided far stronger light-matter interactions as desired for these specific applications. Seeded growth on both Si[9,11] and quartz[12] substrates has been performed by Li *et al.*, overgrowing Ag-NPs of diameters 10-500 nm, with diamond films in the range of 20 – 250 nm. Bellucci *et al.* reported Ag-NP overgrowth on a diamond substrate with 45-65 nm diameter NPs and a 410 nm thick diamond film[10]. Despite varied substrate and growth conditions both Li *et al.* and Bellucci *et al.* reported increased graphitic impurities in grown films with Ag-NPs present. As

for Au-NPs, Nicely *et al.* reported encapsulation in boron doped diamond films for NPs of diameter 100-500 nm[13]. Overall, while successful in other applications, previous studies encapsulating both Ag and Au-NPs in diamond films are too thick for the enhancement field surface projection required for SERS analyte interactions. Additionally, direct comparison of diamond growth interactions around Au and Ag would prove beneficial for further plasmonic diamond studies.

Despite its application for other plasmonic interactions, one which has yet to be explored within diamond films is SERS. Exposed NPs have been paired with diamond surfaces without encapsulation for SERS[14–16]. In these cases the addition of diamond provided further plasmonic enhancement of the Raman signals. However, NPs were still exposed and hence vulnerable to degradation. Fabrication of plasmonic NPs within the diamond film would provide NP protection, negating these longevity issues which have so far prevented real-world application. This study presents a novel investigation of common plasmonic materials (Ag and Au) encapsulated in thin diamond films. Examining their compatibility with thin film diamond growth and ability to produce previously unexplored robust diamond SERS.

The enhancement of interest is present at the diamond-air interface where an analyte would be present. Therefore, there are three parameters which govern the strength of the interaction; distance from the plasmon dipole to the diamond air interface (diamond film thickness), NP material, and NP diameter. It is also desirable to compare the compatibility of different NPs on the diamond growth process, as film quality will also affect the final enhancement.

In this study both Ag and Au-NPs buried in diamond films are investigated, with diameters of $\sim$ 10 nm and $\sim$ 30 nm to allow comparison. Substrate fabrication was performed via annealing deposited metallic films into NPs using a H_2 plasma treatment. Following this diamond was grown around the NPs using Microwave Plasma Chemical Vapour Deposition (MPCVD) before finally reducing diamond film thickness via Reactive Ion Etching (RIE). Substrates have been tested for SERS enhancement with varied NP properties and diamond film thicknesses. Investigation of diamond growth interactions around the Ag and Au-NPs has been undertaken to understand material suitability with respect to fabrication.

Results

Investigation of three substrate fabrication variables was desired: diamond film thickness, NP material (Ag and Au) and NP size. $\sim$ 10 nm and $\sim$ 30 nm NPs were fabricated with both Ag and Au to investigate optimal fabrication parameters. Figure 1 illustrates the substrate fabrication process. Metallic films deposited on SCD (single-crystal diamond) were subsequently annealed into NPs, followed by diamond epilayer growth to facilitate encapsulation, and finally etching to reduce film thicknesses (t). NP sizing for Ag (Figure 1 (a) and (c)) and Au (Figure 1 (b) and (d)) were controlled by varying metallic film deposition thickness, with thicker films resulting in larger NP diameters (d).

The diamond SERS measurement protocol is depicted in Figure 1 (f) whereby (1) analyte must be collected and (2) added to the diamond SERS substrate. (3) Raman spectroscopy measurements may then be performed before (4) removal of the analyte via sonication. The cleaned diamond SERS substrate (5) may then be reused by again adding, measuring and removing the analyte for repeated-use capability.

Nanoparticle Formation

A 4.2 nm Ag film dewetted to NPs with a mean diameter of 10.4 ± 0.3 nm and an inter-particle distance of 5.5 nm. A second Ag film deposition of 9.4 nm and subsequent anneal produced larger NPs within suitably deemed range, with mean diameter 29.6 ± 0.6 nm and an inter-particle gap of 12.5 nm. Regarding Au, a 3.4 nm film was deposited, resulting in a mean NP diameter of 11.0 ± 0.3 nm and inter-particle distance of 6.3 nm. Finally, a thicker Au film of 8.5 nm dewetted to a mean NP diameter of 27.1 ± 1 nm and inter-particle distance of 9.9 nm. Table 1 provides the final fabrication parameters for the metallic NPs.

When analysing the results, a correlation with NP diameter and inter-particle distance can be noted. Due to dewetting mechanisms an increased NP size provides an increased inter-particle distance. Given metallic film dewetting mechanisms on a flat substrate, NPs with a distribution of sizes are produced uniformly across the entire substrate. To obtain the median NP diameter an array of SEM (scanning electron microscopy) images were analysed and the data collated presented in Figure 2. AFM (atomic force microscopy) scans of the fabricated Ag and Au-NPs are given in Figure 3 prior to diamond growth.

Diamond Overgrowth

Growth was performed in steps to enable NP encapsulation tracking. This was conducted via visual and roughness inspection of AFM scans following each growth step. AFM scans for growth on $\sim$ 10 nm and $\sim$ 30 nm NPs can be seen in Figure 3. Additionally, substrate colours were exhibited due to the preferential scattering of light by the fabricated NPs, depicted inset to scans in Figure 3. This colour can be seen to change as the NP's dielectric environment and hence absorption changes with diamond growth. AFM scans also indicate a difference in growth interactions around the NPs of different metallic composition. This is evident when comparing the 10.4 nm Ag-NP film (a) to the 11.0 nm Au-NP film (b) and the 29.6 nm Ag-NP film (c) to the 27.1 nm Au-NP film (d) in Figure 3. Diamond growth over Ag-NPs appears to result in larger grain sizes or growth around

NPs which have moved in the z-direction. It should be noted that AFM scans are unable to distinguish between sp^3 and sp^2 growth so varied structures could be evidence of sp^2 nucleation around Ag-NPs.

Once NPs were deemed encapsulated, substrates underwent a metallic etch process ($\geq$ 30 - $<$ 50% KI, $\geq$ 2.5 - $<$ 10% I_2, 3 minutes), removing any non-encapsulated NPs as well as the Au growth mask. This allowed AFM step measurements to determine diamond epilayer thickness. As a consequence of 160 minutes growth, 108.3 nm and 106.3 nm diamond was grown on the 29.6 nm Ag and 27.1 nm Au-NP substrates respectively. 80 minutes of diamond growth resulted in 20.4 nm growth on the 10.4 nm Ag-NPs and 15.0 nm on the 11.0 nm Au-NPs.

The grown diamond films were investigated with 532 nm excitation Raman spectroscopy to determine crystal quality. Figure 6 (a) provides the collected spectra for each substrate with the initial SCD substrate spectra provided for reference. All spectra have been normalised to the diamond peak which is clearly present at 1331.2 cm^{-1} due to sp^3 lattice vibrations in the diamond crystal[17,18]. An in-depth peak analysis of each film's Raman spectrum is provided in Figure 6 (b-e), with a breakdown of relevant peak assignments is given in Table 2. Further information on the relevant Raman peaks is provided in SI Table S3. Upon peak fitting, it was determined that diamond films grown over Au-NPs provided higher diamond line intensities (11.0 nm Au-NP: 0.981, 27.1 nm Au-NP: 0.972) in comparison to Ag-NPs (10.4 nm: 0.893, 29.6 nm: 0.508) due to greater sp^3 content, where the 27.1 nm Ag-NP film had significantly lower intensity.

Evidence of non-sp^3 disordered carbon can be seen for all grown diamond films given presence of the D-band (peak 4: 1345.8 cm^{-1})[18]. The 29.6 nm Ag-NP substrate contains considerably more disordered carbon than other substrates where the D-band max intensity is 0.259 (Diamond line max intensity = 1). This is followed by films over the 10.4 nm Ag-NPs with D-band intensity of 0.05, where as both Au substrates display further reduction in D-band intensity (11.0 nm Au-NP: 0.02, 27.1 nm Au-NP: 0.03).

Additionally, growth on Ag-NPs resulted in greater graphitic carbon content (peak 6, G-band: 1582.9 cm^{-1})[17,19]. Once more, growth over the 29.6 nm Ag-NPs resulted in the highest portion of graphitic carbon with a G-band max intensity of 0.22, whereas growth over 10.4 nm Ag-NPs provided an G-band intensity of 0.023. Conversely, growth over Au-NPs resulted in minimal graphitic carbon for 11.0 nm Au-NP growth (0.005) and none for 27.1 nm Au-NP growth.

Regarding growth over $\sim$ 10 nm NPs, the presence of microcrystalline graphite (peak 7: 1607.7 cm^{-1}) was identified, unobserved in films grown over the larger $\sim$ 30 nm NPs[20]. More microcrystalline graphite was present in growth over 10.4 nm Ag-NPs (0.023) than in 11.0 nm Au-NP growth (0.004). Further investigation of the 29.6 nm Ag-NP diamond film revealed three additionally Raman peaks not present in other substrates; peak 1, 2 and 5 assigned to transpolyacetylene (at crystal grain boundaries), low-quality diamond and amorphous carbon (I-band) at 1164.7, 1259.0 and 1509.0 cm^{-1} respectively[17,21–24].

Diamond Film Etching

Etches were performed using Kapton tape masks to allow SERS testing of various film thicknesses on the same substrate. Following each etch, the etch depth was measured using AFM. Process times and resulting etch thicknesses are provided in SI Table S1 and S2. Etches were conducted to produce film thicknesses with thin encapsulation of the NPs to enable projection of the SERS enhancement field (produced by excitation of the NPs) to the diamond/air interface. Figures 4 and 5 provide comparable etched diamond film thicknesses for both Ag and Au-NPs. Further AFM and SEM imaging for all diamond film thicknesses are provided in SI Figure S1-S4.

Both the 11.0 nm and 27.1 nm Au-NP substrates exposed NPs as intended upon diamond film etching. Areas appeared relatively smooth with larger Au-NPs breaching the diamond surface at the corresponding film thicknesses as expected. This trend continued until all Au-NPs were exposed, resulting in a comparable structure to that fabricated prior to diamond film growth and etching. All of which indicates no movement of the Au-NPs in the z-direction.

Conversely, movement in the z-direction can be seen for both the 10.4 nm and 29.6 nm Ag-NPs. This is evident in both the AFM and SEM etch images provided in Figures 4 and 5. A significant amount of Ag-NPs breached the surface at much larger diamond film thicknesses than expected, where NP shaping and separation has also changed. Clear evidence of this can be seen for 29.6 nm Ag-NPs with diamond film 54.3 nm and 34.0 nm (Figures 4 and 5 (c)). Upon further etching to fully remove the diamond film a minimal amount of Ag-NPs remained for both size regimes (Figure 5 (a) and (c)). Prior to SERS testing, substrates were exposed to Au etchant ($\geq$ 30 - $<$ 50% KI, $\geq$ 2.5 - $<$ 10% I_2, 3 minutes) to remove all NPs exposed by diamond film etching. Specifically intended for Au etching Ag-NPs are also removed by oxidation of Ag. Any residue was suitably removed by rinsing in DI water to ensure no Raman interference. AFM scans are provided in SI Figure S5 and S6 of etched areas following etchant exposure.

Subsequent to diamond film etching, Raman spectra were captured to investigate diamond quality within the film. These spectra are provided in SI Figure S7. Diamond quality can be correlated with sp^2 to sp^3 ratio comparing the 1582.9 cm^{-1} graphitic carbon peak to the 1331.2 cm^{-1} diamond peak. Graphs displaying this ratio with remaining diamond film thickness are provided in Figure 6 (f) and (g) for $\sim$ 10 nm and $\sim$ 30 nm NP films, respectively. The discrepancy can clearly be seen between Ag-NP and Au-NP diamond overgrowth quality. Growth on Au-NPs leads to a minor increase in sp^2:sp^3 ratio with increasing

film thickness, while the sp^2:sp^3 ratio in diamond growth on Ag-NPs can be seen to increase significantly with thickening diamond film. It should be noted that the films measured are far less than Raman sampling depth. Therefore, the sp^2:sp^3 ratio may be impacted by the changing film thickness given contribution from the underlying SCD substrate, not only the film quality. Thus, less thick films may inherently provide a lower sp^2:sp^3 ratio given their closer proximity to the SCD substrate.

Diamond Encapsulated NP SERS

Following diamond film etching, substrates were functionalised with 1×10^{-4} M Rhodamine 6G (R6G) to investigate SERS enhancement. The captured spectra are provided in Figure 7. Upon excitation with 532 nm, 10.4 nm Ag-NP films provided no resolvable R6G peaks with any diamond film thickness (Figure 7 (a)). Conversely, the 11.0 nm Au-NP diamond substrate produced clearly resolvable peaks with diamond film thicknesses 13.3, 12.0 and 8.7 nm (Figure 7 (b)). These peaks are identified at 612 cm^{-1} as a result of the C-C-C in-plane bending within Rhodamine, and 770 cm^{-1} as a result of C-H out of plane bending[25,26]. R6G peaks in this spectral area were chosen for investigation given their strength and distance from diamond and sp^2 carbon peaks to prevent overlap. Excitation of the 12.0 nm diamond film generated the greatest average 612 cm^{-1} peak intensity and hence optimised film over the 11.0 nm Au-NPs. This is followed by the 13.3 nm and 8.7 nm film thicknesses regarding 612 cm^{-1} intensity. The enhancement capability can be quantified by calculating the enhancement factor (EF). For the 11.0 nm Au-NP substrate the optimised EF = 3.1×10^3 as calculated for the 12.0 nm diamond film (13.3 nm: EF = 2.8×10^3, 8.7 nm: EF = 2.6×10^3). A plot of calculated EF against diamond film thickness for the ~10 nm NP substrates can be seen in Figure 7 (c).

Regarding the substrates with larger ~ 30 nm NPs, both the 29.6 nm Ag-NP and 27.1 nm Au-NP substrates produced evident R6G peaks (Figure 7 (d-e)). Clearly resolvable peaks were present when measuring the 29.6 nm Ag-NPs exclusively at diamond film thickness 54.3 nm, with EF = 5.6×10^3. The 27.1 nm Au-NPs provided the greatest R6G enhancement with peaks present from both the 31.3 and 37.0 nm diamond films. The 31.3 nm exhibited the greatest 612 cm^{-1} intensity and hence EF, with EF = 6.9×10^3 (37.0 nm: EF = 6.0×10^3). Comparison of EF values is given in Figure 7 (f) for ~30 nm NP substrates.

Detection of 1×10^{-4} M R6G with alternative excitation wavelengths was explored to investigate further the spectral response of diamond SERS. Additional to the initial 532 nm excitation, 457 nm, 514 nm and 633 nm were measured for the optimised film thicknesses of 11.0 nm Au-NPs, 29.6 nm Ag-NPs and 27.1 nm Au-NPs. It was found that only 532 nm excites R6G peaks for the 11.0 nm Au-NP and 29.6 nm Ag-NP films. However, with 27.1 nm Au-NPs (31.3 nm film) R6G peaks were clearly resolvable with 514 nm excitation, though with less intensity. R6G was not detected when pairing any diamond SERS with either 457 nm or 633 nm excitation. A spectral set is provided in Figure 8 (a) for the measurement of 27.1 nm Au-NPs (31.3 nm film) at all wavelengths.

Following R6G removal, substrates were exposed to lower concentrations to determine their limit of detection (LOD). Given the inability of the 10.4 nm Ag-NP substrate to detect 1×10^{-4} M R6G it was, of course, unable to detect lower concentrations. However, with optimised etches, the 11.0 nm Au-NP (12.0 nm diamond film), 29.6 nm Ag-NP (54.3 nm diamond film) and 27.1 nm Au-NP (31.3 nm diamond film) NP diamond films provided 1×10^{-5} M detection capability (Figure 8 (b)). A claim of 10 parts per million LOD can be made for these substrates given that the averaged 612 cm^{-1} R6G peak intensities (11.0 nm Au-NP 12.0 nm film: 1098, 29.6 nm Ag-NP 54.3 nm film: 1171, 27.1 nm Au-NP 31.3 nm film: 1316) are greater than three times the blank measurement standard deviation[27]. The standard deviation (11.0 nm Au-NP 12.0 nm film: 54, 29.6 nm Ag-NP 54.3 nm film: 98, 27.1 nm Au-NP 31.3 nm film: 23) is taken from the Raman spectra intensity values of the relevant diamond film measured without analyte. No R6G peaks were present when measuring 1×10^{-6} M, the spectra of which is provided in SI Figure S10.

Given that R6G resonates near to 532 nm an additional analyte control, Methylene Blue (MB), was measured to support the role of substrate spectral response beyond R6G resonance alone. Measurements were taken of $1 \times 10^{-4} - 1 \times 10^{-6}$ M MB on 27.1 nm Au-NPs with 31.3 nm film. As provided in Figure 8 (c), with 532 nm excitation MB was detectable by a pronounced peak at 1626 cm^{-1} (C-C stretch of conjugated rings) for 1×10^{-4} and 1×10^{-5} M matching the LOD for R6G[28]. MB was also measured at 457 nm, 514 nm and 633 nm, for 1×10^{-4} M where the 1626 cm^{-1} was only seen with 514 nm (SI Figure S11), matching the suitable excitation wavelengths for R6G. The absence of a MB peak with 633 nm excitation is notable given MB resonates near to 633 nm (Figure S11), providing evidence that the enhancement mechanism is not solely attributable to R6G resonance effects (and hence is SERS).

Substrate Robustness

To determine diamond SERS substrate longevity and reusability, R6G measurement intensity was investigated following exposure to simulated harsh conditions. Conducted on the etched areas of ~ 30 nm NP substrates which provide the greatest SERS enhancement (29.6 nm Ag-NPs: 54.3 nm diamond, 27.1 nm Au-NPs: 31.3 nm diamond), these tests comprised of sequential exposure to 30 minute sonication, 30 minute Au etchant exposure, 30 minute 400 °C heating in atmosphere and finally 100 sandpaper (3000 grit) abrasion cycles. Following the 400 °C anneal no structural alteration was noted in the Raman

spectrum (SI Figure S12) indicating resistance to combustion at this temperature. Following each exposure, no meaningful change in the 612 cm^{-1} R6G peak intensity was observed, with all variations within the standard error (Figure 8 (d)). As is common practice with Raman measurements, these intensities were adjusted with the a Si reference measurement to account for laser power fluctuations over time. This provides evidence to support the conclusion that diamond SERS is promising for reusable operation whilst providing chemical, thermal, and physical robustness.

Discussion

Robust SERS has been successfully achieved via thin film diamond growth over both Ag and Au-NPs, permitting comparisons regarding performance and fabrication for varied NP sizing and material. Ag and Au-NPs were fabricated on the SCD substrates via a H_2 plasma dewetting mechanism resulting in a distribution of sizing and separation. Median sizing can be controlled through variation of initial metal film thickness, allowing the fabrication of Ag-NPs with median diameter 10.4 and 29.6 nm and Au-NPs of 11.0 and 27.1 nm. This process was chosen due to both its procedural simplicity and compatibility with the following fabrication steps. Given NP formation in the diamond growth chamber future fabrication can be completed consecutively by merely heating the H_2 plasma (to dewet the metal film) then injecting CH_4 to commence diamond growth. Furthermore, utilising this method ensured no alteration to the metallic nanostructures prior to growth.

Alternative plasmonic nanostructures such as nanocubes, nanostars or nanorods could be explored for diamond encapsulation although fabrication temperature must be considered. It is probable that more complex structures would reform into NPs in diamond growth chamber conditions. However, lithography techniques, for example E-beam lithography or nano imprint lithography, would enable templated dewetting on the diamond surface prior to metal deposition. Ultimately further NP fabrication optimisation could be explored to allow greater control regarding NP sizing and separation, however, the additional process complexity, potential diamond film contamination, and chamber condition suitability should be carefully considered[29]. Therefore, currently metallic film dewetting, as established by Li *et al.*[9], is deemed the most suitable approach for this application especially when considering scalability.

For alternate applications, a range of Ag-NP sizing regimes have been reported from 10 nm up to 500 nm in diameter with diamond films ranging from thickness 20 nm, to greater than 400 nm[9–12]. However, regarding Au-NPs just a single report of diamond overgrowth can be found[13]. Nicely *et al.* reported far larger NPs than considered in this study (100 - 500 nm diameter) encapsulated with a thick, 415 nm, boron doped diamond film. Therefore, this study provides unique Au-NP diamond encapsulation of this size regime (2 - 75 nm diameter NPs, $\leq$ 108.3 nm diamond film thickness) and the first investigation to compare Ag and Au-NP diamond encapsulation.

Performing diamond film growth on the fabricated NPs revealed variation in diamond growth mechanisms and quality for the assorted metals and NP sizes. An evident and considerable differentiation can be made regarding the molecular content of diamond film growth incorporating Ag-NPs when comparing to a film incorporating Au-NPs. Ag-NP films were found to contain a far greater proportion of non-diamond formation and, in the instance of Ag-NPs of median diameter 29.6 nm, evidence of non carbon species unique to this substrate (transpolyacetylene, low-quality diamond and amorphous carbon). Ag-NP diamond film growth presented greater inclusion of non sp^3 disordered carbon (D-band) and graphitic carbon (G-band), with the 29.6 nm Ag-NP film exhibiting the greatest non-sp^3 content. Additionally, for both metals a greater non-sp^3 disordered carbon content occurred in the diamond grown over the larger 29.6 nm Ag and 27.1 nm Au-NPs when comparing to the smaller 10.4 nm Ag and 11.0 nm Au-NPs. A number of studies report similar graphitic content (D, I and G-band) with Ag-NP encapsulating diamond films[9,10,12] with Bellucci *et al.* also observing inclusion of transpolyacetylene.

Two main conclusions can be drawn regarding diamond film growth quality over the NPs in this study; greater non-diamond content is produced when growing over (1) Ag-NPs than for Au-NPs and (2) $\sim$ 30 nm NPs than for $\sim$ 10 nm NPs. Moreover, this greater non-diamond content was proven to increase with diamond film thickness (Figure 6 (f) and (g)). This highlights the comparable difference between overgrowth of Ag and Au-NPs, where in the case of this research Ag-NP substrates produced a diamond film of comparably lesser quality. Ultimately, films encapsulating the Au-NPs were found to be of good quality given low indication of non-diamond formation and is notably similar to the initial SCD substrate.

It is believed that this variation between Au and Ag-NP diamond films is be due to movement of Ag-NPs in the z-direction during growth. This could be as a result of the high growth temperature (560 °C) in comparison with the temperature at which Ag-NPs will reform ($\sim$600 °C). The resultant NP reformation and movement during diamond growth interferes with extension of the diamond lattice structure, hence resulting in non-diamond species formation. This Ag-NP movement is further evidenced by the presence of large quantities of exposed Ag-NPs at greater (etched) film thicknesses. Furthermore, upon diamond film growth and subsequent removal via RIE etching, no noticeable alteration from initial Au-NP structures can be seen. Conversely, very little evidence of the initial Ag-NP structure is present when the diamond film is fully removed. This demonstrates the diamond growth and etch processes ability to alter the Ag-NP structures, however, should further pursuit of Ag-NP diamond SERS be of interest, lower temperature growth systems could be considered[30].

Regarding grown diamond film thickness (20.4 nm on 10.4 nm Ag-NPs, 15.0 nm on 11.0 nm Au-NPs, 108.3 nm on 29.6 nm Ag-NPs, 106.3 nm on 27.1 nm Au-NPs) a thinner diamond film growth may be desirable to encapsulate NPs, although, greater growth is required to fully encapsulate purely due to the introduction of the NPs. Given this, it is proposed that this was as a result of excessive growth in the [100] direction either side of NPs before growth in the [110] and [111] directions were induced, resulting in growth far above NP height before encapsulation. This is supported by the AFM scans (Figure 3) where, based upon scan heights, the depth of pits (where NPs are) deepens before substrate surface smoothing during encapsulation.

Upon completion of diamond film etching, the SERS response of areas with varied film thicknesses was investigated with R6G. Given substrate exposure to Au etchant, any NPs exposed via diamond film etching were removed, especially true for the thinnest of diamond films given that the NPs were fully exposed. Therefore, only fully encapsulated NPs remain to contribute to SERS enhancement. As evidenced by Figure 7 no R6G peaks, and hence SERS enhancement, were presented by the 10.4 nm Ag-NP substrate at any film thickness. This could be due to the inability of Ag-NPs of this size regime to stimulate an enhancement field with the ability to project to the diamond-air interface. Alternatively, it may simply be that the diamond growth and etch process has unfavourably modified the Ag-NP structures.

However, the larger 29.6 nm Ag-NPs successfully exhibited SERS enhanced R6G peaks for a single diamond film thickness of 54.3 nm (EF = 5.6 $\times 10^3$). Enhancement for only the diamond film of this thickness and no others further evidences that Ag-NPs migrate in the z-direction during diamond growth. Conversely, both Au-NP substrates presented SERS enhancement for multiple diamond film thicknesses. 11.0 nm Au-NPs enhanced the R6G analyte with diamond film thicknesses 8.7, 12.0 and 13.3 nm where 12.0 nm provided the greatest with EF = 3.1 $\times 10^3$. The 27.1 nm Au-NPs provided R6G enhancement with film thicknesses 31.3 and 37.0 nm where the 31.3 nm film provided the larger enhancement with EF = 6.9 $\times 10^3$. Therefore, this 31.3 nm thick epilayer over 27.1 nm diameter Au-NP diamond film provided the optimised enhancement of the substrate configurations tested.

Whilst gap effects between NPs can dominate SERS signal intensity with exposed NPs this can be assumed to be very minor or insignificant due to prevention of analyte interaction between NPs by the diamond film. The diamond film encapsulating the NPs assures a monolayer of analyte above the NPs when performing measurements. Given AFM and SEM characterisation was comprehensive across the area of substrates, the median diameter and inter-particle distance of the plasmonic enhancing NPs was taken as uniform across the substrate prior to growth. However, large-area SERS spatial uniformity was not fully quantified in this study, therefore, future work should include Raman mapping or measurements over a large grid of points to investigate this. Without this, maintained NP morphology throughout growth and diamond film thickness were the main considerations for fabrication at this stage.

When examining the optimised enhancement structure in this study it can be considered that the main parameter reducing enhancement is the analyte-NP distance. Given encapsulation of NPs in diamond, the minimum analyte-NP distance is at the diamond film surface. The distance dependence of SERS can be quantified using Eq. 1[31]. Where a is NP radius and r is the analyte-NP surface distance. For the optimised enhancement structure NPs are 27.1 nm in diameter ($a = 13.55$ nm) encapsulated in 31.3 nm diamond film ($r = 4.2$ nm). This provides a theoretical SERS intensity of 6.7% of the intensity at the NP surface. This may then be reduced further by the diamond dielectric, however, it should be noted that diamond is known to have a very low attenuation coefficient at 532 nm (≤ 0.1 cm^{-1}[32]). Local thickness is assumed to be uniform and flat when evaluating AFM and SEM characterisation. However, film thickness measurements are taken from AFM step measurements at etch area edges, so uniformity is challenging to ensure. Should thickness variations occur this would of course influence the effective analyte-NP distance.

$$I_{SERS} = \left(\frac{a+r}{a}\right)^{-10} \tag{1}$$

It is feasible that control of the diamond film roughness may provide greater enhancement mechanisms and surface hot spot density, especially given diamond light scattering qualities[14–16,33]. This may be done through altered growth parameters or post growth intentional roughening techniques. However, this could compromise film quality and adversely impact optical properties of the system.

The diamond film thickness providing greatest enhancement for each substrate (excluding 10.4 nm Ag-NPs, 12.0 nm on 11.0 nm Au-NPs, 54.3 nm on 29.6 nm Ag-NPs, 31.3 nm on 27.1 nm Au-NPs) were then tested with R6G of lower concentrations where a LOD was determined of 1×10^{-5} M. This is of course incomparable to the pinnacle of paper-based SERS with R6G LOD down to 1×10^{-11} M[34], though diamond-based SERS provides reusability and real-world environmental deployment suitability while remaining applicable for automated fabrication. Nevertheless, the LOD reported here is comparable to commercially available SERS substrates, all whilst the NPs are encapsulated within the diamond films[35].

Varying laser wavelength demonstrated enhancement capability with both 532 nm and 514 nm excitation for R6G. However, 532 nm provided a greater signal intensity indicating substrate resonance closer to 532 nm and hence is the most suitable

excitation for diamond encapsulated SERS. Furthermore, the detection of MB provided evidence that enhancement does not exclusively rely on analyte resonance effects. This is given that excitation wavelengths supporting the detection of MB match those for R6G (532 nm, 514 nm).

Diamond SERS films then underwent chemical, thermal and physical robustness testing to determine their reusability via exposure to extended sonication, extended Au etchant, 400 °C in atmosphere and 3000 G sandpaper abrasion. No perceptible change in SERS enhancement potential was observed, ultimately proving the robustness of the diamond SERS platform for application in previously unobtainable SERS application areas. It should be emphasised that all repeated measurement tests were conducted on the same substrate areas, with no degradation following analyte removal and repeated exposure suggesting reliable substrate reusability. This reusable diamond SERS measurement protocol is depicted in Figure 1 (f).

Previous approaches towards robust SERS substrates have been reported with steel wire mesh[4], SiO_2 coatings[5], nickel foam-cages[6], copper foam coatings[7], boron nitride coatings[8] and diamond-like carbon coatings (DLC)[36,37]. Each addressed certain SERS robustness challenges where the steel wire mesh (laser beam heat dissipation), SiO_2 coating (900 °C tested) and boron nitride coating (700 °C tested) provided thermal resistance to varying degrees. Although only tested to 400 °C in this study, diamond has been shown to resist oxidation to > 700°C in atmosphere, meaning diamond SERS substrates should also be suitable for use in very high temperatures[38].

Additionally, the boron nitride coatings enabled the possibility to reuse the substrate multiple times following exposure to 15% nitric acid in water, indicating a similar level of chemical resilience as diamond SERS. However, SiO_2 and boron nitride coatings are unable to address physical robustness issues. If only oxidation resilience is of concern, DLC coatings have been reported to provide oxidation resilience to Ag-NPs whilst producing further SERS enhancement. Although substrate resilience is yet to be investigated for DLC coated SERS.

Nickel foam-cages addressed physical robustness, exhibiting the ability to withstand sandpaper abrasion (3000 G). Although initial SERS signal reduction was observed (3%) from abrasion, no further reduction in enhancement was observed with further abrasive cycles. Furthermore, nickel foam-cage SERS substrates resisted damage from sonication (30 mins) with only minor signal reduction (12%). Copper foam coatings reported a similar signal drop after 100 sandpaper abrasion cycles (14%). Here, the diamond SERS substrates exhibited no loss of SERS intensity following equal abrasion and sonication procedures, proving its superior physical robustness.

Overall, while previous research has independently addressed certain SERS challenges, none have achieved a fully robust system. Moreover, regarding practical durability, other reports towards robust SERS were performed on fragile substrate materials. The substrates presented here are covered entirely in diamond, addressing all longevity and durability concerns. Diamond provides a chemically, physically and thermally resilient platform, enabling truly robust and reusable SERS measurements for almost any setting.

Conclusion

This study provides the first comprehensive comparison of the suitability of the two most reported plasmonic metals, Ag and Au, for incorporation in thin diamond films. These films were assessed regarding their application as robust and reusable SERS substrates with the detection of a common test analyte, R6G. Evidence has been provided to support the conclusion that Au-NPs are preferable to Ag-NPs. Ag-NPs induced far greater non-diamond formation during film deposition, appearing to shift in the z-direction. This introduced fabrication challenges where their durability during growth and subsequent etching is doubtful. Additionally, regarding application for SERS sensing, Au-NPs for both sizing regimes ($\sim$ 10 nm and $\sim$ 30 nm median diameter) provided greater analyte enhancement. Au-NPs of median diameter 27.1 nm evidenced the optimised enhancement in a diamond film of thickness 31.3 nm, providing an EF = 6.9 $\times 10^3$ and LOD of 1×10^{-5} M. The plasmonic diamond films were then assessed regarding robustness and reusability, demonstrating capability to endure sonication, Au etchant, 400 °C (atmosphere) and 3000 G sandpaper abrasion. This replicates and surpasses previously reported SERS substrate resilience all whilst preventing any degradation in SERS response. Further to this, continued use of substrates via sonicated solvent analyte removal demonstrates promising reusable SERS operation, providing comparable enhancement to commercially available substrates. This work greatly improves on the current state of reusable and robust SERS substrates with promising application potential in laboratory measurements and beyond.

Materials and Methods

This research employed $4 \times 4 \times 0.3$ mm optical grade single crystal diamond {100} substrates (2 side polished) (Chenguang Machinery). An initial cleaning step was performed via submersion in an acid solution (20 g $(NH_4)_2S_2O_8$) : 20 ml H_2SO_4, 200 °C, 20 minutes) and subsequent rinse solution (10 ml H_2O_2 : 10 ml H_5NO, 10 minutes) to ensure removal of undesired surface compounds[39].

Primary substrate characterisation measurements were performed via Raman spectroscopy (Renishaw InVia Raman Spectrometer, 532 nm excitation) and atomic force microscopy (AFM) (Bruker Dimension Icon). Subsequently an Au asymmetric film (∼100 nm) was sputtered (Lesker PVD75) on the substrate corners to provide a masked area for diamond deposition measurements. This Au film is of a thickness greater than which would dewet with H_2 plasma treatments, ensuring it will remain continuous, preventing diamond growth in the desired area.

Nanoparticle Formation

The fabrication of metallic NPs was enabled via metallic deposition and subsequent anneal. Ag deposition on the prepared diamond substrates was conducted via physical vapour deposition (Edwards A306 Metal Box evaporator) from Ag wire. Following deposition, exposure to air drives Ag oxidation, however this can be disregarded due to burn off during the annealing (and diamond growth) process. The deposition of Au films on diamond was conducted via sputter coating (EMscope SC500). Deposited film thickness for Au and Ag were varied to control dewetted NP characteristics.

Following this the deposited films were then dewetted into NPs through a H_2 plasma annealing process (Seki Technotron AX5010 diamond growth reactor). Au and Ag films were both annealed using the same conditions. To avoid the evaporation of Ag (∼600 °C), the plasma was heated to 560 °C. Plasma heating was conducted to this temperature and then immediately decreased via control of pressure and microwave power.

Scanning electron microscopy (SEM) (Carl Zeiss XV1540) was performed to investigate subsequently formed NPs (Figure 2). To minimise oxidisation prior to characterisation, samples with Ag-NPs were subjected to minimal air exposure. Subsequent SEM images were analysed using ImageJ analysis software to determine NP diameter and inter-particle distance. To determine the inter-particle distance (edge to edge) an ImageJ plugin, ND (nearest distances), was used[40].

Both the SEM images and AFM scans indicated that the dewetting process was influenced by the presence of surface defects on the substrate, such as polishing lines. As such, a flatter surface is preferred for uniform dewetting. Not all NPs appear to be fully spherical in the 2D plane, potentially due to the uneven nature of the substrate, as a result of the trenches. However, investigation of AFM scans confirmed that the majority of NPs are of approximately the same height as diameter across, confirming their spherical nature.

Diamond Overgrowth

Diamond film growth to encapsulate NPs was performed with a Seki Technotron AX5010 diamond growth reactor. A base pressure of 2×10^{-5} mBar was used for each growth with additional H_2 flushes to evacuate the chamber of contaminants. Growth was conducted at 560 °C with a microwave power of 625 w and 35 Torr pressure. To enable precise, high quality diamond growth a gas mixture of 0.25% CH_4 in H_2 was used (0.5:199.5 sccm).

Raman spectroscopy was used to investigate the grown films using a Renishaw InVia Raman system with 532 nm excitation (0.45 mW). Spectra collected over five 20s accumulations were averaged over three different random position measurements across the substrates. In OriginPro software the resultant spectra underwent asymmetric least squares baseline subtraction (Asymmetric Factor = 0.0001, Threshold = 0.001, Smoothing Factor = 9, Number of Iterations = 10) to remove background fluorescence. No additional smoothing or cosmic ray removal was performed. Following baseline subtraction spectra were normalised to 1 and analysed with origin fit peaks function using Gaussian peak shapes and auto fit control. An example of fluorescence subtraction and peak fitting is provided in SI Figure S8.

Diamond Film Etching

Diamond films were then etched to investigate the influence of film thickness and obtain the optimised conditions for SERS measurements. Diamond etching was achieved using O_2 plasma RIE (reactive ion etching). Based on previously reported shallow etching, 200 W was used to generate an O_2 plasma with 40 sccm oxygen flow in 10 Pa[41].

SERS Enhancement Testing

Following diamond film etching, substrate SERS enhancement was investigated using Rhodamine 6G (R6G) (Merck, 99% purity) at a concentration of 1×10^{-4} M. Substrates were exposed to the R6G solution for 10 minutes, rinsed with DI water and dried with N_2. Each measurement consisted of five accumulations of 20 s exposure with a Renishaw InVia Raman system at 1% power (457 nm: 0.3/30 mW, 514 nm: 0.5/50 mW, 532 nm: 0.45/45 mW, 633 nm: 0.3/30 mW). In this set-up the laser beam is collimated, expanded and then coupled into the microscope. The beam is focused onto the SERS surface by a 20× Olympus microscope objective (NA = 0.75) leading to a diameter of 865 nm. Backscattered Raman is collected by the same microscope objective, optically filtered, dispersed and analysed by a highly sensitive CCD detector. In this collection a diffraction grating is utilised with 2400 lines/mm. Fluorescence was subtracted by asymmetric least squares baseline subtraction (Asymmetric Factor = 0.001, Threshold = 0.01, Smoothing Factor = 3, Number of Iterations = 10) in OriginPro software. An example of fluorescence subtraction is provided in SI Figure S9. No additional smoothing or cosmic ray removal was performed. R6G intensity values were averaged from 612 cm^{-1} peak height of three different random position measurements across areas of interest and standard

error calculated from the three measurements. To determine substrate limit of detection (LOD), measurements were taken of further diluted R6G with concentration 1×10^{-5} M and 1×10^{-6} M. Additionally, Methylene Blue (MB) (Merck, $\geq 97\%$ purity) was utilised to investigate SERS response at a concentration of $1 \times 10^{-4} - 1 \times 10^{-6}$ M using the same preparation method as for R6G. Analyte removal was conducted via consecutive sonication in methanol, acetone and IPA (5 minutes each) when required.

SERS enhancement was then quantified via Enhancement Factor (EF) calculations with Eq. (2)[31]. In this equation I_{SERS} represents SERS intensity, I_{Raman} the standard Raman intensity (both taken from the 612 cm^{-1} R6G raman peak), N_{SERS} the number of molecules near the SERS nanostructure and N_{Raman} the molecules in the volume which gives rise to I_{Raman}. Additionally, Re_{SERS} and Re_{Raman} represent an Si reference taken to account for equipment variability. An example of such calculation is provided in SI.

$$EF = \frac{I_{SERS}/N_{SERS}}{(I_{Raman}/N_{Raman}) \times \frac{Re_{SERS}}{Re_{Raman}}} \tag{2}$$

Substrate Robustness Measurements

Finally, to examine robustness and reusability, substrates were sequentially exposed to simulated harsh conditions. 30 minutes sonication (Guyson Kerry KC2 ultrasonic bath) in DI was conducted, followed by extended Au etchant exposure for 30 minutes. Following this, to establish thermal stability, substrates were exposed to 400 °C for 30 minutes in atmosphere conditions by means of hotplate (Thermic Edge). Substrates were then subjected to sandpaper abrasion from 3000 grit sandpaper to ascertain physical robustness. A 20 g weight was affixed to the substrates underside with carbon tape to providing a force of 1.25 g mm^{-2}. Without applying extra pressure to the weight substrates were manually pushed 10 cm along the sandpaper repeatedly for 100 cycles. Following each harsh condition exposure R6G 1×10^{-4} M was added to enable SERS measurements. Subsequent to this the R6G was removed via solvent sonication then re-added following the next harsh condition exposure.

Acknowledgements

The authors are grateful to the UKs Engineering and Physical Sciences Research Council (EPSRC) and SLB Cambridge Research Ltd for the award of a CASE PhD studentship (EP/W524335/1)to KNT, supervised by RBJ. Dr Calum S. Henderson is thanked for his manuscript proofing. He and Dr Rebecca J. Watkins are thanked for their advice throughout fabrication and analysis. Undergradute student Edward Young is thanked for his aid in nanoparticle characterisation. The LCN cleanroom are acknowledged for the invaluable assistance of technicians with the AFM, SEM and evaporation tools respectively. The Royce Imperial cleanroom is also acknowledged for assistance with Reactive-ion etching (RIE).

Author Contributions

R.B.J. and M.L.A.R supervised all aspects. M.L.A.R., K.N.T. and R.B.J conceived the ideas behind the study. K.N.T. carried out the substrate fabrication, characterisation, data collection, analysis, manuscript preparation and submission.

References

1. Lee, S.-T., Lin, Z. & Jiang, X. Cvd diamond films: nucleation and growth. *Mater. Sci. Eng. R: Reports* **25**, 123–154, DOI: 10.1016/S0927-796X(99)00003-0 (1999).
2. Liu, Y. *et al.* Evaluation of the reliability of six commercial sers substrates. *Plasmonics* **15**, 743–752, DOI: 10.1007/s11468-019-01084-8 (2020).
3. Vandenabeele, P. *Practical Raman Spectroscopy – An Introduction* (John Wiley and Sons Ltd, 2013).
4. Szymborski, T. *et al.* Steel wire mesh as a thermally resistant sers substrate. *Nanomaterials* **8**, DOI: 10.3390/nano8090663 (2018).
5. Liu, M. *et al.* Fabrication, characterization, and high temperature surface enhanced raman spectroscopic performance of sio2 coated silver particles. *Nanoscale* **10**, 5449–5456, DOI: 10.1039/C7NR08631H (2018).
6. Vu, T. D., Duy, P. K. & Chung, H. Nickel foam–caged ag-au bimetallic nanostructure as a highly rugged and durable sers substrate. *Sensors Actuators B: Chem.* **282**, 535–540, DOI: 10.1016/j.snb.2018.11.098 (2019).
7. Bui, T. T. *et al.* Highly durable and reusable 3d copper foam-based sers substrate with cuo-ag nanorods for ultrasensitive measurements of rhodamine-6g and human urine. *ACS Appl. Nano Mater.* **8**, 844–853, DOI: 10.1021/acsanm.4c06298 (2025).

8. ul Ahmad, A. *et al.* Cheap, reliable, reusable, thermally and chemically stable fluorinated hexagonal boron nitride nanosheets coated au nanoparticles substrate for surface enhanced raman spectroscopy. *Sensors Actuators B: Chem.* **304**, DOI: https://doi.org/10.1016/j.snb.2019.127394 (2020).

9. Li, S., Bandy, J. & Hamers, R. J. Enhanced photocatalytic activity of diamond thin films using embedded ag nanoparticles. *ACS Appl. Mater. Interfaces* **10**, 5395–5403, DOI: 10.1021/acsami.7b13821 (2018).

10. Bellucci, A. *et al.* Plasmonic silver nanoparticles facilitate electron emission from diamond upon sun-like excitation. *ChemPhotoChem* **9**, DOI: 10.1002/cptc.202400202 (2025).

11. Li, S. *et al.* Ag diamond core shell nanostructures incorporated with silicon vacancy centers. *ACS Mater.* **2**, 85–93, DOI: 10.1021/acsmaterialsau.1c00027 (2022).

12. Li, S., Bandy, J. & Hamers, R. J. Tunable coloration of diamond films by encapsulation of plasmonic ag nanoparticles. *Diam. Relat. Mater.* **89**, 190–196, DOI: 10.1016/j.diamond.2018.09.003 (2018).

13. Nicley, S. S. *et al.* Growth of boron doped diamond films on gold coated substrates with and without gold nanoparticle formation. *Cryst. Growth Des.* **19**, DOI: 10.1021/acs.cgd.9b00488 (2019).

14. Song, J. *et al.* A novel surface-enhanced raman scattering substrate: Diamond nanopit infilled with gold nanoparticle. *Mater. Lett.* **135**, 214–217, DOI: 10.1016/j.matlet.2014.07.139 (2014).

15. Song, J., Li, H., Cheng, S. & Wang, Q. Fabrication of a hybrid structure of diamond nanopits infilled with a gold nanoparticle. *RSC Adv.* **60**, 32000–32003, DOI: 10.1039/C4RA03196B (2014).

16. Li, Y., Duan, W. & Wei, J. Synthesis of diamond@sio2@ag composite materials for high sers effect. *Ceram. Int.* **47**, 16870–16875, DOI: 10.1016/j.ceramint.2021.02.262 (2021).

17. Zaitsev, A. M. *Optical Properties of Diamond: A Data Handbook* (Springer Berlin, Heidelberg, 2001), 1 edn.

18. S., P. & J., N. R. Raman spectroscopy of diamond and doped diamond. *Philos Trans A Math Phys Eng Sci.* **362**, 2537–2565, DOI: 10.1098/rsta.2004.1451 (2004).

19. J., N. R. Growth and characterization of diamond thin films. *Annu. Rev. Mater. Sci.* **21**, 535–558, DOI: 10.1146/annurev.ms.21.080191.002535 (1991).

20. Jackman, R. B., Beckman, J. & Foord, J. S. Diamond chemical vapor deposition from a capacitively coupled radio frequency plasma. *Appl. Phys. Lett.* **66**, 1018–1020, DOI: 10.1063/1.113591 (1995).

21. Ferrari, A. C. & Robertson, J. Origin of the $1150-\mathrm{cm}^{-1}$ raman mode in nanocrystalline diamond. *Phys. Rev. B* **63**, 121405, DOI: 10.1103/PhysRevB.63.121405 (2001).

22. Bou, P. & Vandenbulcke, L. Raman investigations on diamond films and crystals deposited by plasma-assisted cvd. *J. Electrochem. Soc.* **138**, 2991–3000, DOI: 10.1149/1.2085354 (1991).

23. López-Ríos, T., Sandré, E., Leclercq, S. & Sauvain, E. Polyacetylene in diamond films evidenced by surface enhanced raman scattering. *Phys. Rev. Lett.* **76**, 4935–4938, DOI: 10.1103/PhysRevLett.76.4935 (1996).

24. Yoshikawa, M. *et al.* Characterization of crystalline quality of diamond films by raman spectroscopy. *Appl. Phys. Lett.* **55**, 2608–2610, DOI: 10.1063/1.101951 (1989).

25. He, X. N. *et al.* Surface-enhanced raman spectroscopy using gold-coated horizontally aligned carbon nanotubes. *Nanotechnology* **23**, 1–9, DOI: 10.1088/0957-4484/23/20/205702 (2012).

26. Hildebrandt, P. & Stockburger, M. Surface-enhanced resonance raman spectroscopy of rhodamine 6g adsorbed on colloidal silver. *The J. Phys. Chem.* **88**, 5935–5944, DOI: 10.1021/j150668a038 (1984).

27. Bzik, T. J. *"Detecting the Detection Limit," in Detection Limits in Air Quality and Environmental Measurements* (West Conshohocken, PA: ASTM International, 2019).

28. Horta, I. *et al.* Ultra-trace monitoring of methylene blue degradation via agnw-based sers: Toward sustainable advanced oxidation water treatment. *Sustainability* **17**, DOI: 10.3390/su17104448 (2025).

29. Rane, A. V., Kanny, K., Abitha, V. & Thomas, S. *Synthesis of Inorganic Nanomaterials*, chap. 5: Methods for Synthesis of Nanoparticles and Fabrication of Nanocomposites, 121–139 (Woodhead Publishing, 2018).

30. Stiegler, J., Lang, T., Nygard-Ferguson, M., von Kaenel, Y. & Blank, E. Low temperature film growth limits by microwave plasma-assisted cvd. *Diam. Relat. Mater.* **5**, 226–230, DOI: 10.1016/0925-9635(95)00349-5 (1996).

31. Stiles, P. L., Dieringer, J. A., Shah, N. C. & Duyne, R. P. V. Surface-enhanced raman spectroscopy. *Annu. Rev. Anal. Chem.* **1**, 601–626, DOI: 10.1146/annurev.anchem.1.031207.112814 (2008).

32. Webster, S. *et al.* Intrinsic and extrinsic absorption of chemical vapor deposition single-crystal diamond from the middle ultraviolet to the far infrared. *J. Opt. Soc. Am. B* **32**, 479–484, DOI: 10.1364/JOSAB.32.000479 (2015).

33. Jiang, L. *et al.* Selective sers detection of tatb explosives based on hydroxy terminal nanodiamond-multilayer graphene substrate. *ACS Omega* **9**, 22166–22174, DOI: 10.1021/acsomega.4c00749 (2024).

34. Wei, W. *et al.* Cellophane paper-based surface-enhanced raman scattering (sers) substrates for detecting rhodamine 6g in water and chili powder. *Vib. Spectrosc.* **102**, 52–56, DOI: 10.1016/j.vibspec.2019.04.004 (2019).

35. Azziz, A., Safar, W., Xiang, Y., Edely, M. & de la Chapelle, M. L. Sensing performances of commercial sers substrates. *J. Mol. Struct.* **1248** (2022).

36. Liu, F., Cao, Z., Tang, C., Chen, L. & Wang, Z. Ultrathin diamond-like carbon film coated silver nanoparticles-based substrates for surface-enhanced raman spectroscopy. *ACS Nano* **4**, 2643–2648, DOI: https://doi.org/10.1021/nn100053s (2010).

37. Washek, C. C., Murcia-Correa, L. S., Bonetti, L. F., Corat, E. J. & Trava-Airoldi, V. J. Dlc based substrate enabling single molecule detection by surface enhanced raman spectroscopy (sers). *Diam. Relat. Mater.* **151**, DOI: https://doi.org/10.1016/j.diamond.2024.111775 (2025).

38. Sun, Y. *et al.* Enhancement of oxidation resistance via titanium boron carbide coatings on diamond particles. *Diam. Relat. Mater.* **92**, 74–80, DOI: 10.1016/j.diamond.2018.12.019 (2019).

39. Baral, B., Chan, S. S. M. & Jackman, R. B. Cleaning thin-film diamond surfaces for device fabrication: An auger electron spectroscopic study. *J. Vac. Sci. & Technol. A: Vacuum, Surfaces, Films* **14**, 2303–2307, DOI: 10.1116/1.580063 (1996).

40. Haeri, M. & Haeri, M. H. M. Imagej plugin for analysis of porous scaffolds used in tissue engineering. *J. Open Res. Softw.* **3**, DOI: 10.5334/jors.bn (2015).

41. Huang, T.-Y. *et al.* A monolithic immersion metalens for imaging solid-state quantum emitters. *J. Vac. Sci. & Technol. A: Vacuum, Surfaces, Films* **10**, 2392, DOI: 10.1038/s41467-019-10238-5 (2019).

Graphical Abstract

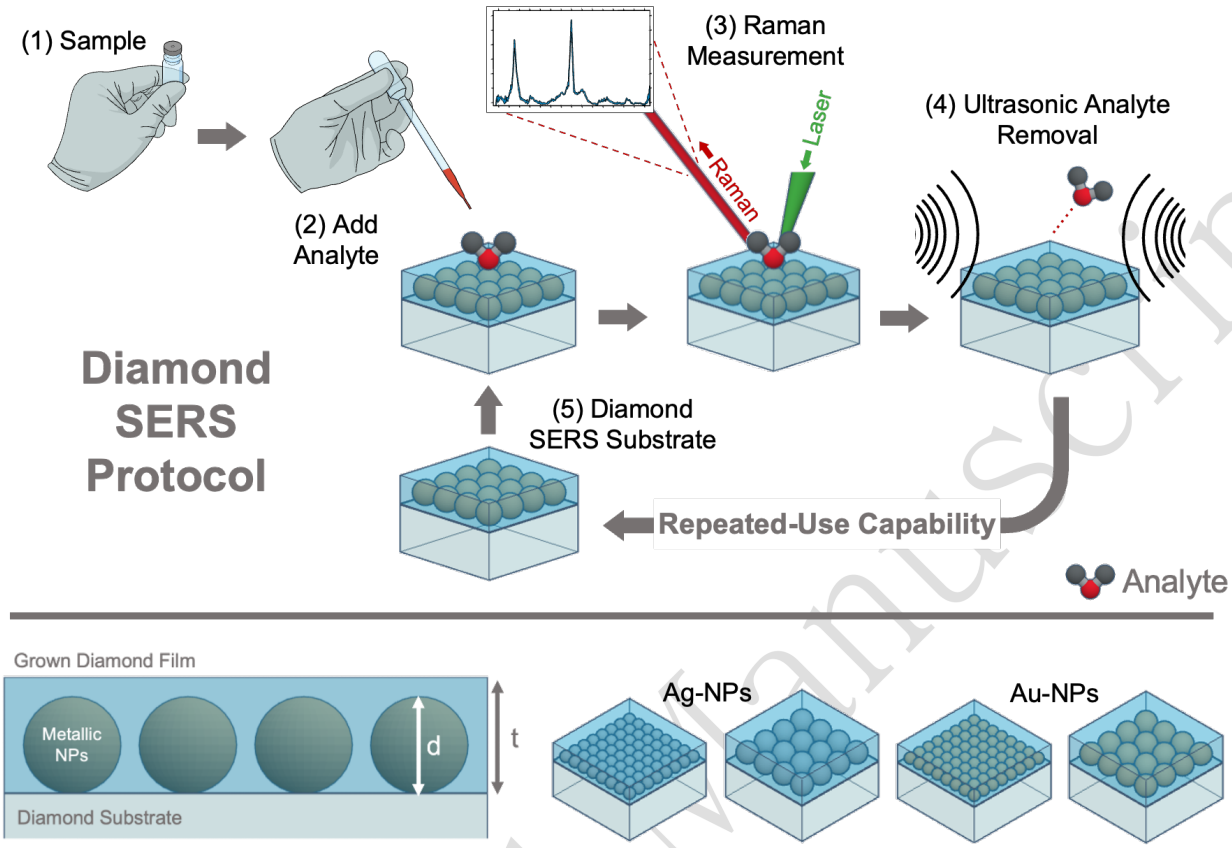

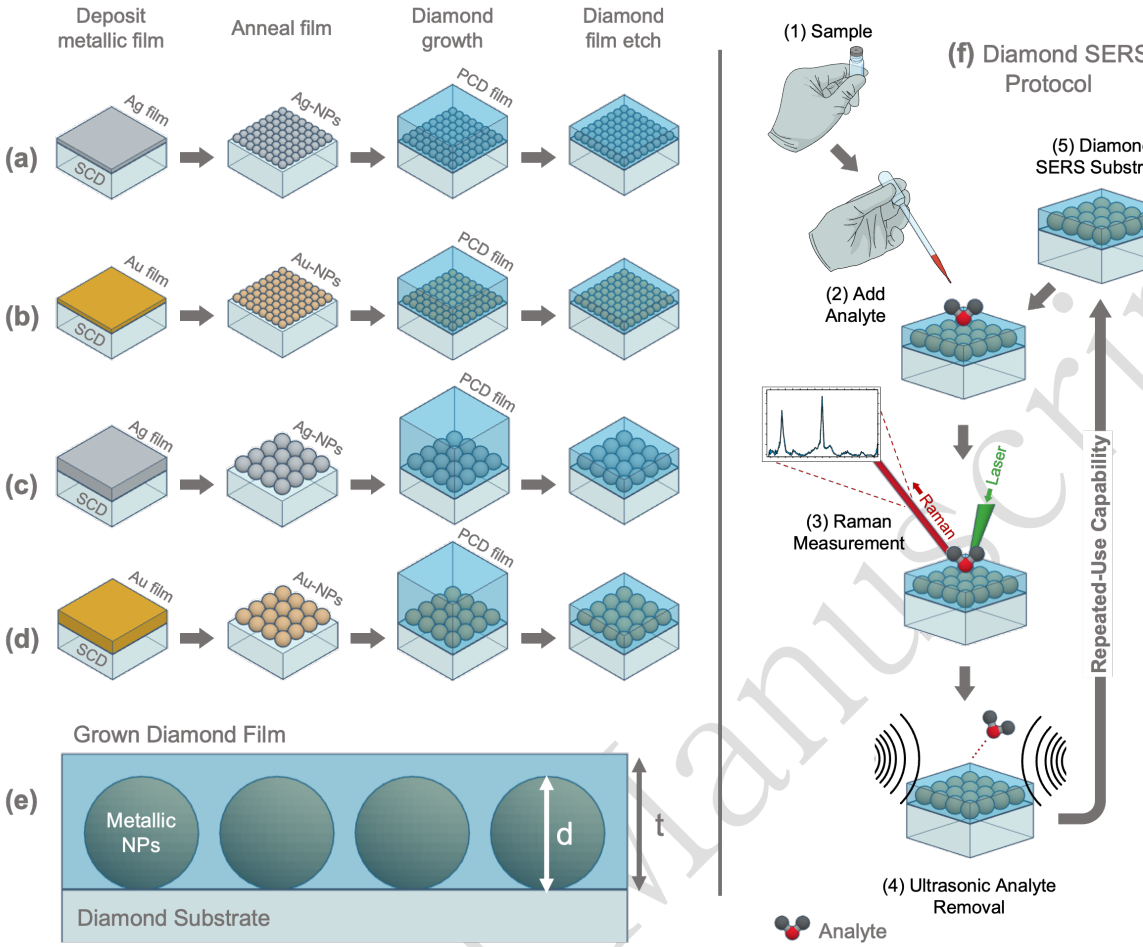

Figure 1. Diamond SERS substrate fabrication process flow. Fabrication process for (a) 10.4 nm Ag-NP substrate (b) 11.0 nm Au-NP substrate (c) 29.6 nm Ag-NP substrate (d) 27.1 nm Au-NP substrate. Single Crystal Diamond (SCD) substrates undergo deposition of a thin film of Au or Ag varying thickness to control NP sizing, H_2 plasma anneal to form NPs, Polycrystaline diamond (PCD) film overgrowth and finally diamond film etching. (e) cross section depiction of desired substrate fabrication where d is NP diameter and t is grown diamond film thickness. (f) depicts the diamond SERS measurement protocol whereby (1) analyte must be sampled and (2) added to the diamond SERS substrate. (3) Raman spectroscopy measurements may then be performed before (4) removal of the analyte via sonication. The cleaned diamond SERS substrate (5) may then be reused by again adding, measuring and removing the analyte for repeated-use capability.

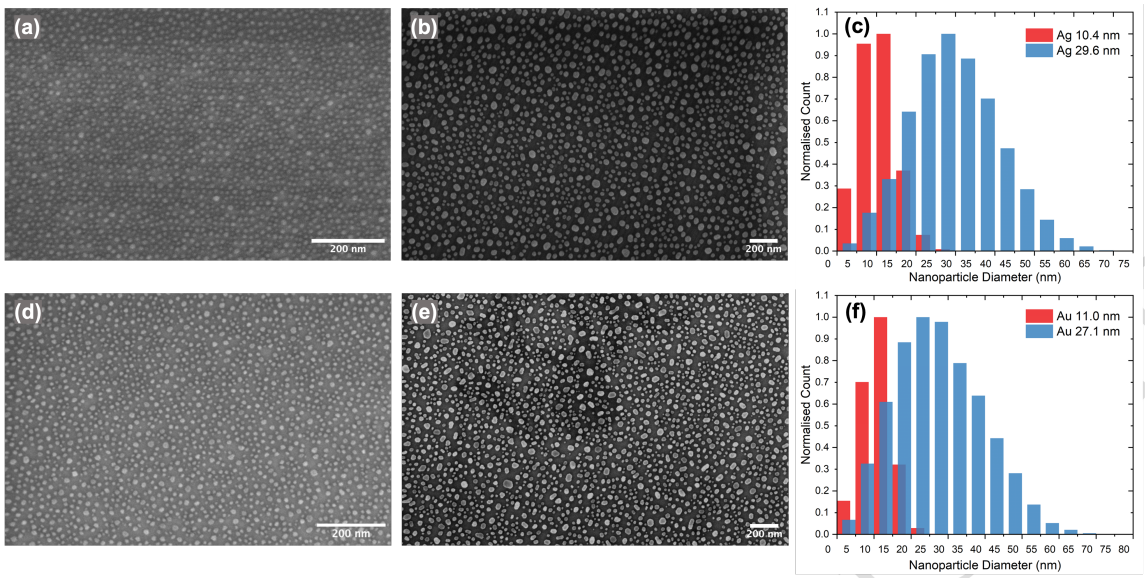

Figure 2. Metallic nanoparticles (NPs) fabricated from dewetting thin films on diamond. SEM of Ag-NPs of average diameter (a) 10.4 nm and (b) 29.6 nm. (c) Normalised bar graph of Ag nanoparticle diameter sizing distribution. SEM of Au-NPs of mean diameter (d) 11.0 nm and (e) 27.1 nm. (f) Normalised bar graph of Au nanoparticle diameter sizing distribution.

Table 1. NP fabrication results.

Metal	**Ag**		**Au**	
Film thickness (nm)	4.2	9.4	3.4	8.5
Median NP diameter (nm)	10.4	29.6	11.0	27.1
Median inter-particle distance (nm)	5.5	12.5	6.3	9.9

Table 2. Diamond film Raman peak assignments.

Peak	**Position (cm^{-1})**	**Assignment**
1	1164.7	Transpolyacetylene at grain boundaries[21]
2	1259.0	Low-quality diamond[17,22]
3	1331.2	Diamond line[17,18]
4	1345.8	D-band: non sp^3 disordered carbon[18]
5	1509.0	I-band: amorphous carbon[23,24]
6	1582.9	G-band: graphitic carbon[17,19]
7	1607.7	Microcrystalline graphite[20]

Table 3. Enhancement factors of Ag and Au-NPs diamond films with varied film thicknesses.

Substrate	**Diamond Film Thickness**	**EF**
10.4 nm Ag-NPs	-	-
11.0 nm Au-NP	8.7 nm	2.6×10^3
	12.0 nm	3.1×10^3
	13.3 nm	2.8×10^3
29.6 nm Ag-NPs	54.3 nm	5.6×10^3
27.1 nm Au-NP	31.3 nm	6.9×10^3
	37.0 nm	6.0×10^3

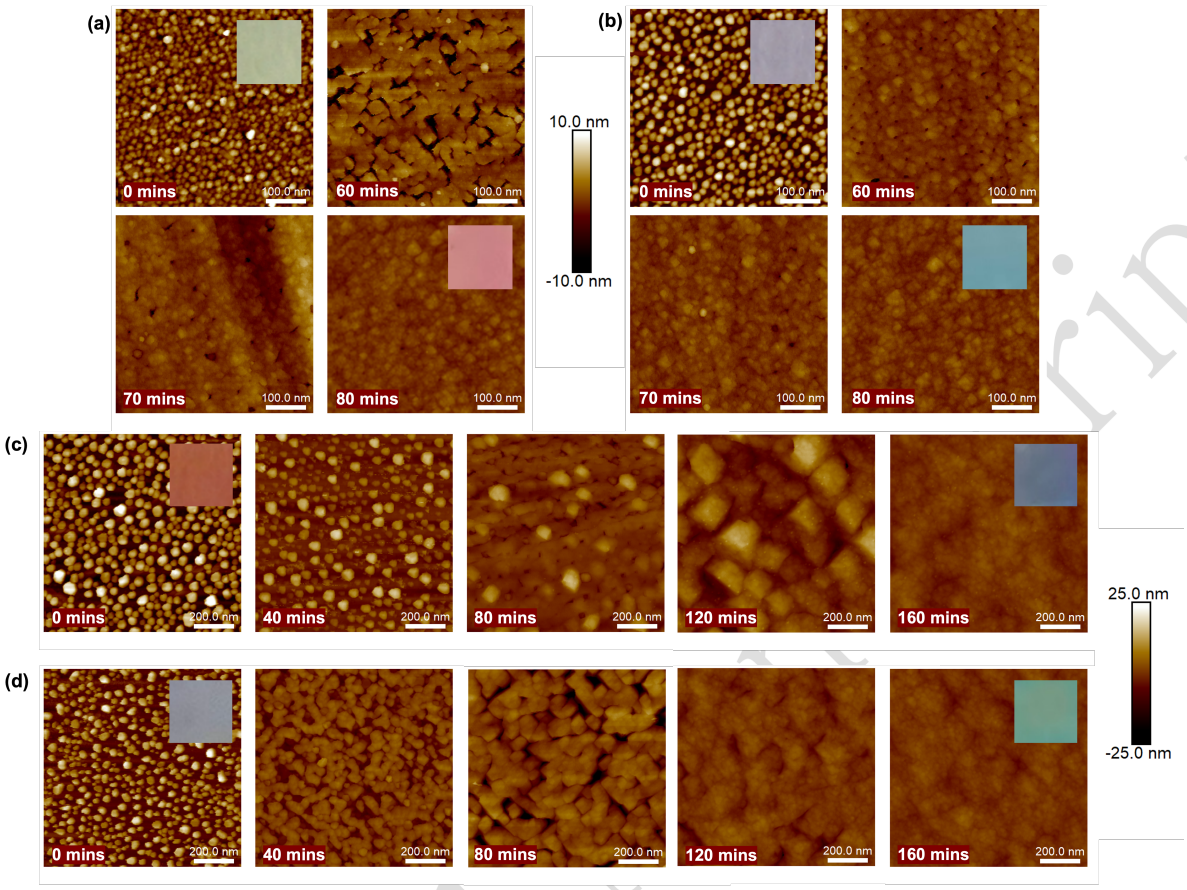

Figure 3. 1 μm AFM scans of diamond growth over (a) 10.4 nm Ag-NPs (b) 11.0 nm Au-NPs (c) 29.6 nm Ag-NPs (d) 27.1 nm Au-NPs, growth times are provided inset to images. Inset: differing substrate colours are provided due to preferential scattering of light (daylight) by fabricated metallic NPs on diamond substrates. Colour can be seen to change when exposed NPs are encapsulated by diamond overgrowth.

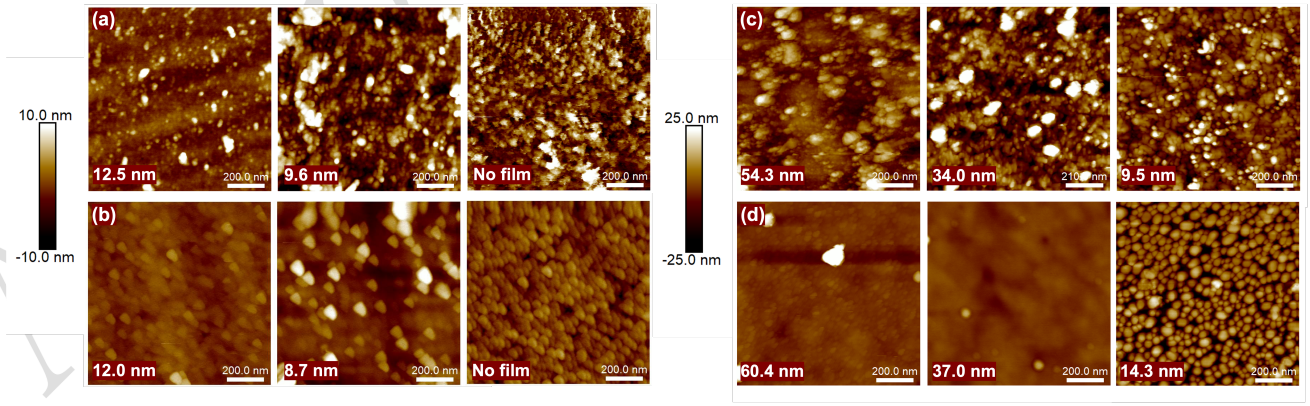

Figure 4. 1 μm AFM scans of etched diamond films over (a) 10.4 nm Ag-NPs (b) 11.0 Au-NPs (c) 29.6 nm Ag-NPs (d) 27.1 nm Au-NPs. Remaining diamond film thicknesses are provided inset to images with etching conducted until diamond film is fully removed.

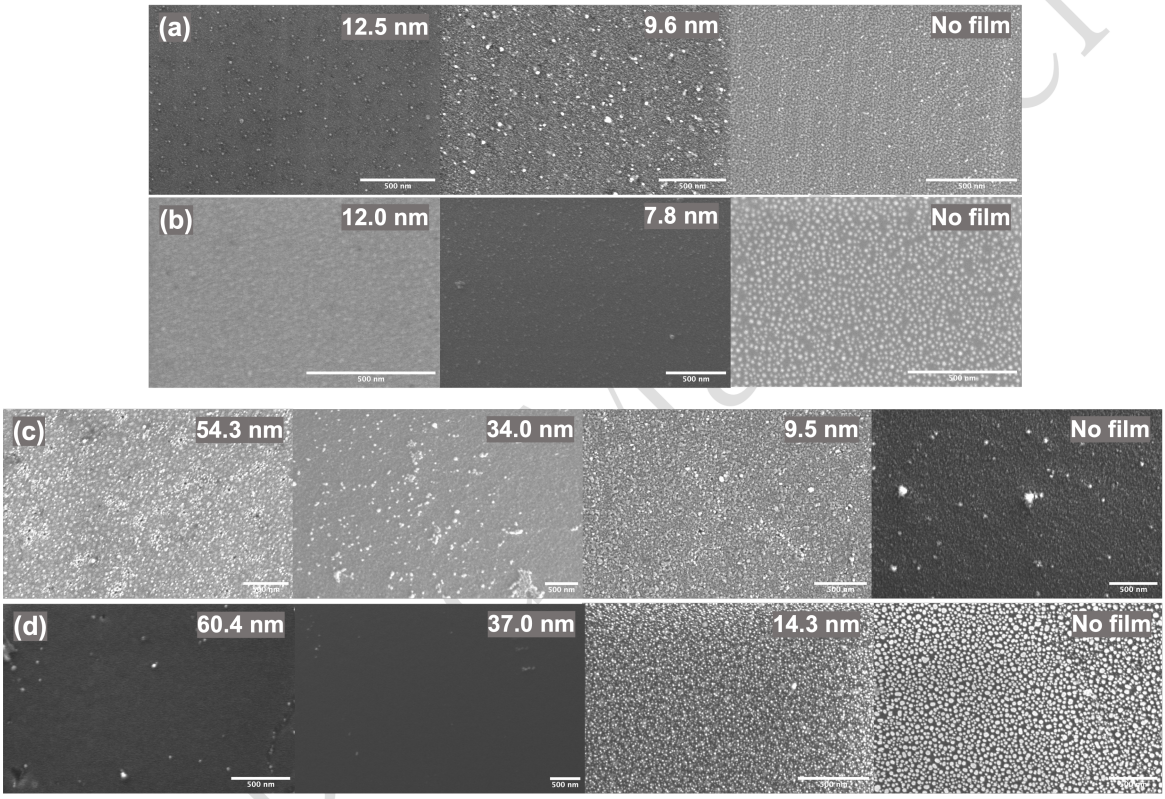

Figure 5. SEM images of etched diamond films over (a) 10.4 nm Ag-NPs (b) 11.0 Au-NPs (c) 29.6 nm Ag-NPs (d) 27.1 nm Au-NPs. Remaining diamond film thicknesses are provided inset to images with etching conducted until diamond film is fully removed.

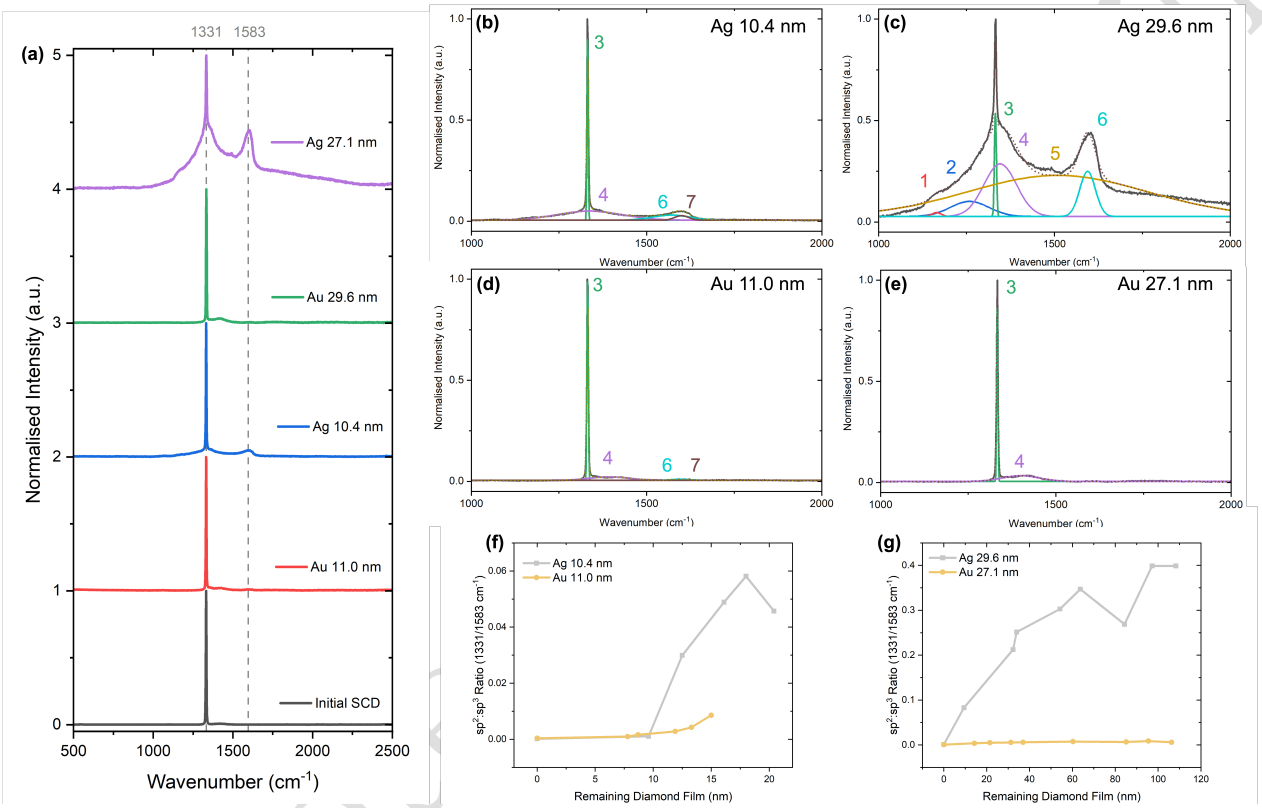

Figure 6. Carbon content of diamond films encapsulating metallic NPs (a) Normalised Raman spectra of grown diamond films subjected to 532 nm excitation where prominent peaks can be seen at 1332 cm^{-1} (sp^3 diamond peak) for all substrates. Spectra offset in y to facilitate comparison. Peak fitting of Raman spectra is provided for diamond films over (b) 10.4 nm Ag-NPs (c) 29.6 nm Ag-NPs (d) 11.0 nm Au-NPs (e) 27.1 nm Au-NPs. Graphs displaying sp^2 to sp^3 ratio comparing the 1582.9 cm^{-1} graphitic carbon peak to the 1331.2 cm^{-1} diamond peak with respect to diamond film thickness for (f) $\sim$ 10 nm and (g) $\sim$ 30 nm diameter NP films.

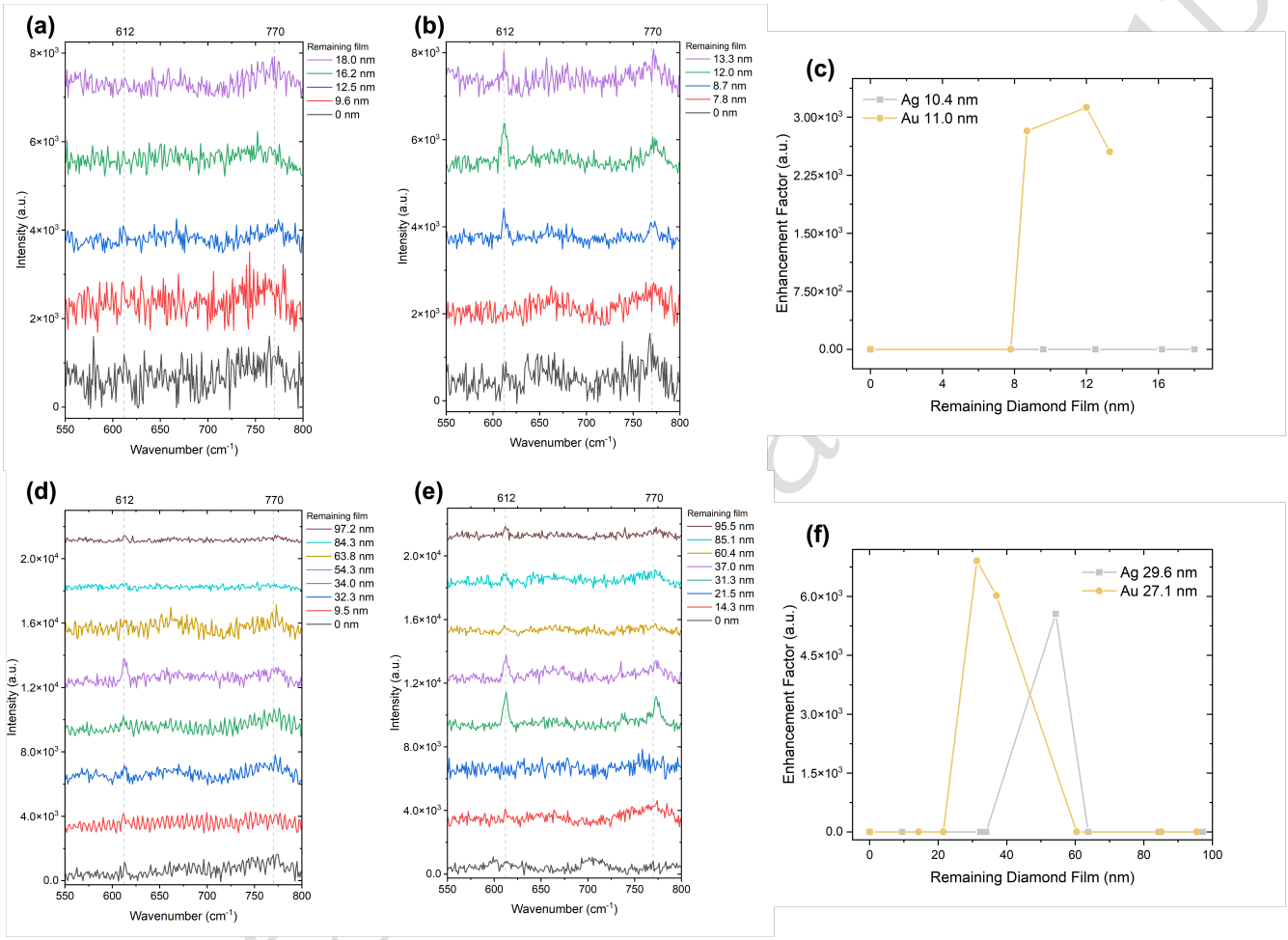

Figure 7. Raman spectra of 1×10^{-4} M R6G on diamond SERS substrates with (a) 10.4 nm Ag-NPs (b) 11.0 nm Au-NPs (d) 29.6 nm Ag-NPs (e) 27.1 nm Au-NPs when excited with 532 nm. Spectra from varied diamond film thicknesses can be seen offset in y with R6G peaks present at 612 cm^{-1} and 770 cm^{-1}. Enhancement Factors calculated from these measurements are provided in (c) and (f) for $\sim$ 10 nm and $\sim$ 30 nm diameter NP films respectively.

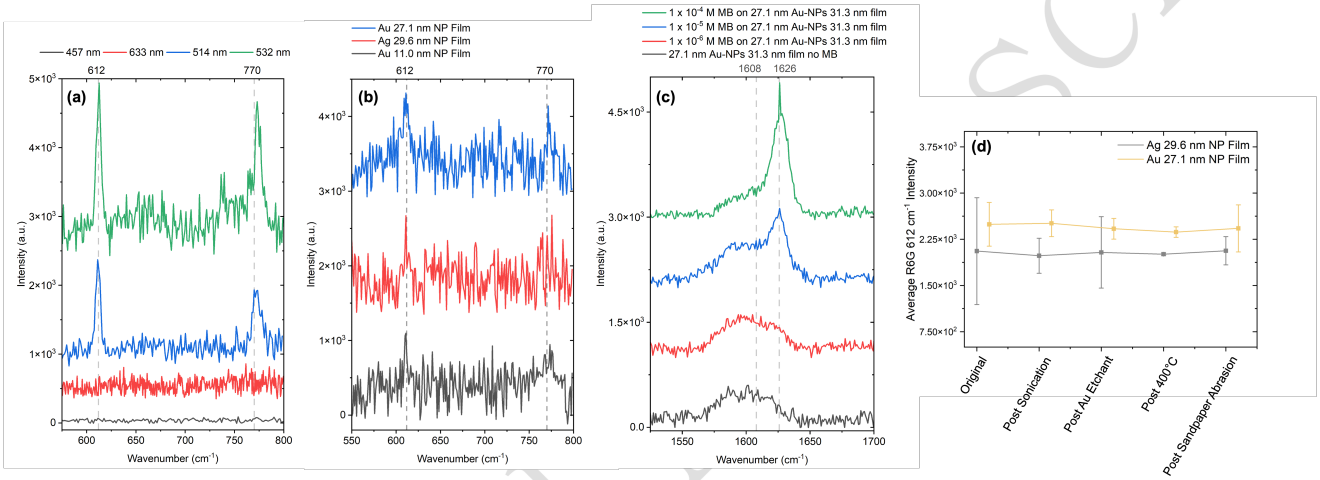

Figure 8. (a) Raman spectra of 1×10^{-4} M R6G on 27.1 nm Au-NPs with 31.3 nm diamond film at varied excitation wavelengths of 457 nm, 514 nm, 532 nm and 633 nm with spectra offset in y. (b) Substrates limit of detection of 1×10^{-5} M R6G with 532 nm excitation. Spectra is provided for the etched areas of substrates which provide the greatest SERS enhancement (11.0 nm Au-NPs: 12.0 nm diamond, 29.6 nm Ag-NPs: 54.3 nm diamond, 27.1 nm Au-NPs: 31.3 nm diamond) offset in y. R6G peaks can be seen at 612 cm^{-1} and 770 cm^{-1}. (c) Raman spectra of $1 \times 10^{-4} - 1 \times 10^{-6}$ M MB on 27.1 nm Au-NPs with 31.3 nm film (532 nm excitation). A pronounced peak at 1626 cm^{-1} for 1×10^{-4} and 1×10^{-5} M indicates MB. A secondary broad peak at 1608 cm^{-1} indicates a minor inclusion of microcrystalline graphite in the film. (d) Averaged 612 cm^{-1} R6G peak intensity following robustness tests of sequential extended sonication, exposure to Au etchant, 400 °C heating and 100 sandpaper abrasion cycles. Standard error bars are provided where negligible Raman intensity variation from the original can be seen, all within the standard error.